1

Introduction

"It is difficult to admit the existence of molecules in interstellar space because when once a molecule becomes dissociated there seems no chance of the atoms joining up again."
—Sir Arthur Eddington

Life on Earth arose at least 3.7 billion years ago, when our planet was approximately 700 Myr old (Mojzsis *et al.*, 1996; Hassenkam *et al.*, 2017). This time estimate comes from biogenic carbon inclusions found in the oldest known terrestrial rocks, the Isua rocks in West Greenland. Although upper limits on *when* life appeared are available, it is still very uncertain *how* life emerged in the Universe, and in particular what were the exact physical conditions triggering the transition from chemistry to biology. In this context, astronomical observations of young solar-type stars can yield valuable insights onto the environment and reactions at play during the birth of planetary systems akin to our Solar System. Comparisons between the molecular species detected around young stars and found in pristine meteorites, comets and asteroids, provide important clues on the chemical evolution leading to the origin of life in the early Solar System and potentially elsewhere in the Universe.

What we currently know about life is that it appeared as the product of complex chemical reactions leading to stable biomolecules assembling into cells and, ultimately, multicellular organisms (Ehrenfreund and Charnley, 2000). A logical key step consists of tracing what are the ingredients required for the synthesis of biomolecules when solar-type stars are born. From astronomical observations and theoretical models, we can ascertain that gas-phase and solid-state chemistries are intertwined and promote chemical complexity during the assembly of a planetary system (e.g., Herbst and van Dishoeck, 2009; Jørgensen *et al.*, 2020; Öberg and Bergin, 2021). The subtle interplay between these two phases of matter is involved in the formation of diatomic molecules such as molecular hydrogen (H_2), to the production of the building blocks of life in planetary systems. The study of this interplay is fundamental to unveil the intricate chemical steps that brought simple molecules to give rise to larger biomolecules and, ultimately, to the primordial metabolism on early Earth.

The work presented in this thesis investigates the solid-gas interplay in protostellar envelopes surrounding low-mass protostars. The main aim is to test how different physical conditions impact the balance between gas-phase and solid-state chemistries, and in a broader context, how this affects the composition of the material incorporated into forming-planets. To accomplish this goal, this thesis is driven by comparative studies of gas and solid interstellar molecules at millimeter and infrared wavelengths, respectively.

The main focus of this is methanol (CH_3OH). Methanol is a prime test-case as according to models and laboratory experiments, it predominantly forms as a consequence of the solid-gas interplay (hydrogenation of condensed CO molecules onto the grain surfaces) and it is associated with the production of more complex molecules. To explore how the environment influences the balance between gas and solid-state chemistries, observational constraints on the gas-to-ice ratios of CH_3OH are calculated in nearby star-forming regions located in three different giant molecular clouds.

This thesis is structured as follows. Chapter 1 gives an introduction to the present view of the star-formation process, based on recent astronomical observations, theoretical predictions and simulations. In particular, it provides an overview of the evolutionary stages of the formation of a low-mass star, focusing on the solid and gas-phase composition of the material involved in this journey. The remainder of the chapter describes our current knowledge of the gas-phase and solid-state chemistries at work in pre- and protostellar environments, setting the initial conditions for planet formation.

Chapter 2 outlines the methods adopted in this thesis. It begins with a summary of molecular spectroscopy, focusing on the dominant transitions characterizing molecular spectra of star-forming regions. It continues with a description of astronomical observations of solid-state and gas-phase interstellar molecules at infrared and millimeter wavelengths. The chapter ends with an introduction to the basic principles of radio-interferometry, and to the combination of single-dish and interferometric data.

Chapter 3 presents the three low-mass star-forming regions selected as testbeds for the presented research: the Serpens cloud core, the Orion Barnard 35A cloud and the Coronet cluster in Corona Australis. It starts with a presentation of the giant molecular cloud complexes and it continues with a brief, more detailed characterization of the physical structure of the star-forming clusters.

Chapter 4 summarizes the articles forming an integral part of this thesis. It discusses their contribution to the field of astrochemistry and proposes some avenues for future work. The articles themselves are presented in Chapters 5, 6, and 7.

1.1 THE FORMATION AND EVOLUTION OF A LOW-MASS STAR

The journey of the solid-state and gas-phase material leading to the formation of a low-mass star starts in dense regions of the InterStellar Medium (ISM), called *Giant Molecular Clouds* (GMCs). These are large asymmetric structures with sizes on the order of ≈100 pc and masses ≈ $10^5 M_\odot$ (Herbst and van Dishoeck, 2009; Heyer and Dame, 2015). Table 1.1 summarizes the typical densities and temperatures of these environments. The vast majority of their mass is in the form of molecular gas, although a smaller fraction (approximately 1 % of the total mass) is locked in micrometer-size dust grains mostly composed of silicates and refractory carbon-bearing compounds (Draine, 2003; Henning, 2010).

Inside giant molecular clouds reside higher density regions with sizes of ≈0.1 pc, called *dense cores*. The average dense core density is a few 10^4 cm^{-3} and the temperature is ≈10 K (Myers *et al.*, 1983; Benson and Myers, 1989; Bergin and Tafalla, 2007). Dense cores tend to form along filamentary structures (e.g., Schneider and Elmegreen, 1979; Myers, 2009; André *et al.*, 2010; Könyves *et al.*, 2015) which originate as a consequence of the cloud turbulent activity compressing the molecular gas (Padoan and Nordlund, 2002; Mac Low and Klessen, 2004; André *et al.*, 2014). Figure 1.1 shows one of the most notable examples of filamentary networks, observed in the Polaris flare cloud.

Pre-stellar cores can undergo gravitational collapse, initiating a cascade of processes leading to the formation of a star, and eventually of a planetary system. In the classical description of star formation, the core is approximated as an isothermal sphere of gas with a density profile following the power-law $\rho \propto r^{-2}$ at larger radii and flattening at small radii. The maximum mass the core can have to be gravitationally bounded is referred to as the mass of a *Bonnor-Ebert sphere* ($M_{\rm BE}$) (Ebert, 1955; Bonnor, 1956):

$$M_{\rm BE} = \frac{C_{\rm BE} c_{\rm s}^4}{\sqrt{P_0 G^3}} \tag{1.1}$$

where the constant $C_{\rm BE}$ is ~1.8, $c_{\rm s}$ represents the isothermal sound speed, P_0 is the pressure of the gas and G is the gravitational constant. When the mass of the core exceeds the critical mass of the Bonnor-Ebert sphere, the core begins to collapse in free-fall from the central regions, characterized

TABLE 1.1: Comparison between densities and temperatures in interstellar, circumstellar and planetary environments. The density is expressed as hydrogen nuclei per cm^{-3}.

Environment	n(cm^{-3})	T(K)	Object
Giant Molecular Cloud	100	15	Orion
Dark Cloud	500	10	Taurus-Auriga
Dense Core	10^4	10	TMC-1
Disk midplane*	$10^6 - 10^{11}$	10 – 150	T-Tauri
Planet	†10^{19}	300	Earth

Note: Adapted from Stahler and Palla (2004). * from Williams and Best (2014). † molecules per cm^{-3}.

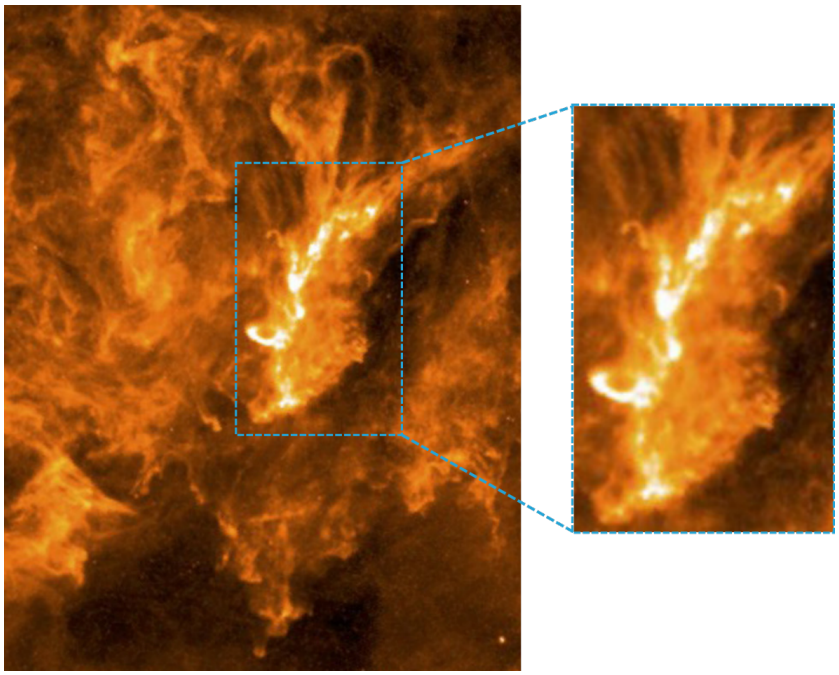

FIGURE 1.1: *Herschel*/SPIRE 250 μm image capturing the filamentary structure of the Polaris flare cloud. The zoom-in displays the brightest filament which harbours multiple non-spherical dense cores. Adapted from André (2017).

by the highest densities. The density profile within the collapse radius, corresponding to the free-falling inner *protostellar envelope* regions, follows the power-law $\rho \propto r^{-1.5}$. This inflow region expands radially at the sound speed until the accretion front reaches the external layers of the core. Since the expansion occurs from the inner to the outer layers of the cloud core, this model is called the *inside-out collapse* (Shu, 1977).

In general, the inside-out collapse provides a good conceptual understanding of the low-mass star-formation process, but it does not necessarily account for the full physical picture. For instance, modern-day high resolution observations (e.g., Lin *et al.*, 2017; Zhang *et al.*, 2020) and detailed numerical simulations (Kuffmeier *et al.*, 2017; Bate, 2018) have shown that cores are not spherical as assumed by classical calculations (Jeans, 1902), but inherit more complex structures from the large-scale environment as can be seen in Figure 1.1. Additionally, stars often form in clusters (Duquennoy and Mayor, 1991; Tobin *et al.*, 2015; Murillo *et al.*, 2016), as it is the case for the protostars studied in Chapters 5, 6 and 7.

The sequence of events implicated in the formation and evolution of a protostar entails multiple physical processes, many of which are only partially understood and challenged by observations and computational simulations. Figure 1.2 displays a simplified illustration of such processes. After the collapse has begun, more and more material accreates towards the center of the core. When the material reaches densities and temperatures sufficiently high ($T \approx 10^6$ K) for deuterium fusion reactions to ignite, a protostar forms at the center. The infalling material carries the angular momentum of the parental core. Due to the conservation of angular momentum, a portion of material settles into a *circumstellar disk* around the protostar (Tscharnuter, 1975; Terebey *et al.*, 1984). The presence of a large-scale

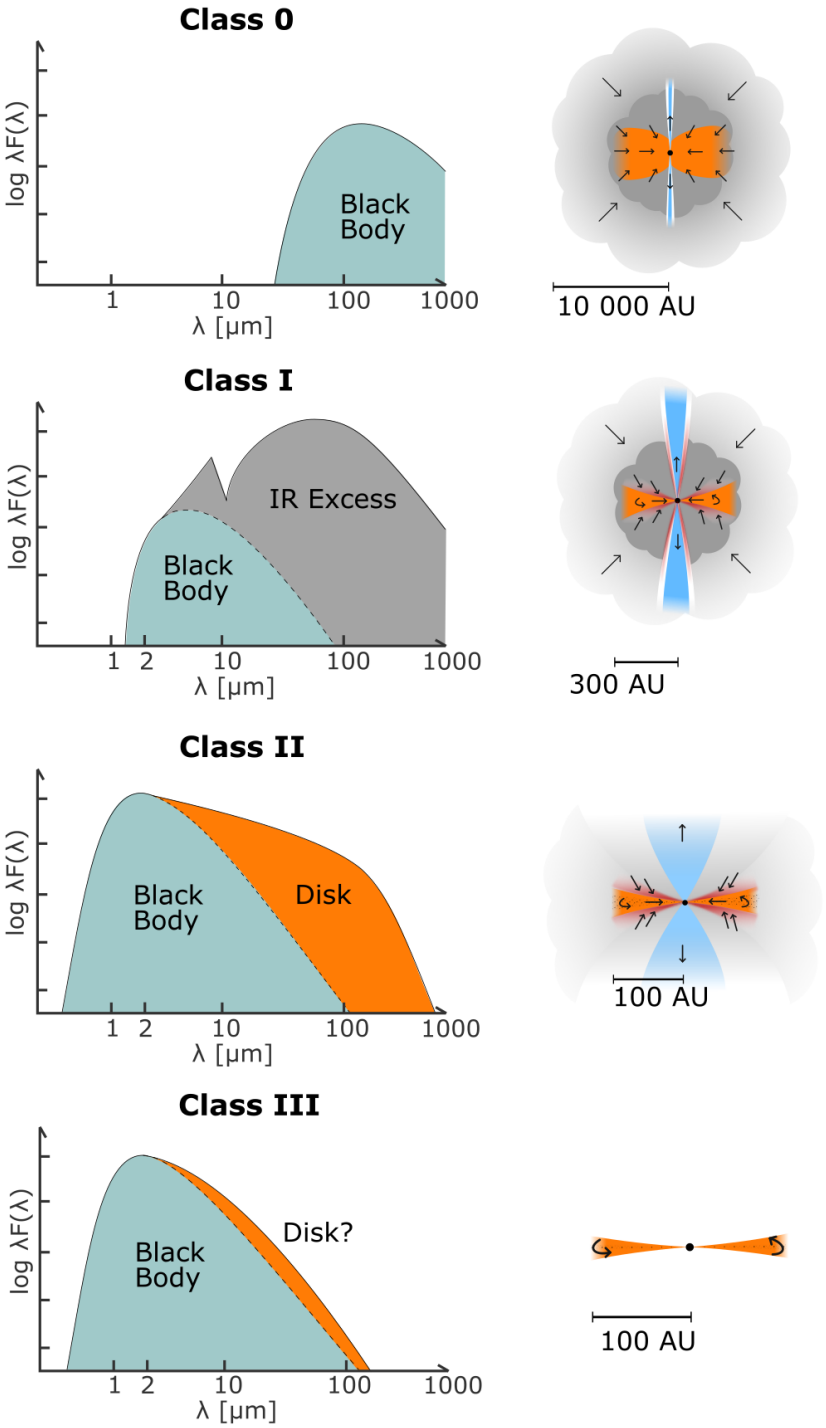

FIGURE 1.2: Evolutionary stages of low-mass young stellar objects. *Left:* Spectral energy distributions (SEDs). *Right:* Cartoon representing each protostellar stage. Credit: M. V. Persson.

magnetic field regulates the rotation of the disk (Pudritz and Ray, 2019). It can remove angular momentum from the protostar-disk system through powerful outflows such as jets and winds (Blandford and Payne, 1982) and via a process called magnetic braking (Lüst and Schlüter, 1955; Mestel, 1968).

The circumstellar disk is commonly referred to as *protoplanetary disk*, to indicate that it is the birthplace of planets. Disks lifetimes are typically on

TABLE 1.2: Physical quantities used to classify young stellar objects.

Class	SED slope (α_{IR})	Bolometric temperature (T_{bol})	Luminosity ratio (L_{submm}/L_{bol})
0	-	$T_{bol} \leq 70$ K	> 0.5 %
I	$\alpha_{IR} > 0.3$	70 K $< T_{bol} \leq 650$ K	< 0.5 %
II	-1.6 $< \alpha_{IR} <$ -0.3	650 K $< T_{bol} \leq 2800$ K	-
III	$\alpha_{IR} <$ -1.6	$T_{bol} > 2800$ K	-

Note: Adapted from Williams and Cieza (2011). The values for the bolometric temperature and L_{submm}/L_{bol} are taken from Chen *et al.* (1995) and Dunham *et al.* (2014), respectively.

the order of 1 – 10 Myrs (Mamajek, 2009; Williams and Cieza, 2011). In this period of time, the aggregation of dust grains in the disk interior forms pebbles of bigger and bigger sizes which ultimately lead to the assembly of planetary embryos, and eventually planets (Brauer *et al.*, 2008; Blum and Wurm, 2008). It is still not completely clear when exactly planet formation occurs, but recent high-resolution observations of young disks suggest that planets start to assemble earlier than previously thought, possibly already during the embedded (Class 0/I) stages of the young stellar object (ALMA Partnership *et al.*, 2015; Andrews *et al.*, 2018; Harsono *et al.*, 2018; Alves *et al.*, 2020).

1.1.1 *The earliest protostellar classes: Class 0 and Class I*

The evolution of young stellar objects have traditionally been captured through classification of them based on their *spectral energy distributions* (SEDs). Figure 1.2 displays the SEDs and the illustration of the corresponding protostellar class. Initially, the young protostars were catalogued into three classes, Class I-III, according to the slope of their spectral energy distributions at near- and mid-infrared wavelengths (Lada, 1987). A decade later, a second classification was introduced which, compared to the previous grouping, added an earlier class, the "Class 0" (Andre *et al.*, 1993). When moving from Class 0 to Class III, the spectral energy distribution curve is shifted to shorter wavelengths (Fig. 1.2), reflecting the dispersal of the protostellar envelope and, later in the evolution, of the circumstellar disk.

Young stellar objects are classified according to:

- their *infrared spectral index* (α_{IR}) = $\frac{\mathrm{d}\log(\lambda F_\lambda)}{\mathrm{d}\log(\lambda)}$, which represents the slope of the SED in logarithmic scale in the spectral range between 2.2 and 20 μm (Lada, 1987);

- their *bolometric temperature* (T_{bol}), i.e., the temperature of a black body with the same mean frequency as the observed continuum spectrum (Myers and Ladd, 1993);

- the ratio between the luminosity at submillimeter wavelengths ($\lambda \geq$ 350 μm) and the bolometric luminosity L_{submm}/L_{bol} (Dunham *et al.*, 2014). This identifier was introduced to discriminate between Class 0 and Class I sources.

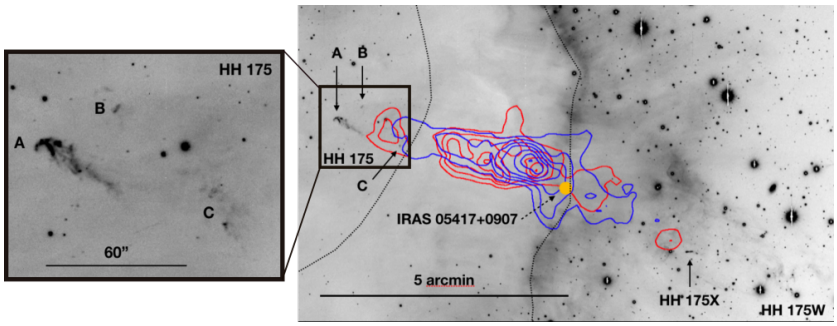

FIGURE 1.3: The molecular outflow driven by IRAS05417+0907 overlaid on a [SII] optical image. The bright clumps of the Herbig-Haro 175 can be observed towards the end of the eastern lobe of the outflow, to the left of the image. Credit: Reipurth and Friberg (2021).

Table 1.2 delineates the conventional values adopted to classify young stellar objects. In general, this classification provides a broad picture of the nature of the individual sources. However, it is important to remark that the classes do not directly reflect the physical stage of an object (Robitaille *et al.*, 2006), as shown by synthetic observations based on MHD simulations of collapsing giant molecular clouds (Frimann *et al.*, 2016) and actual observations of the earliest stellar stages (e.g., Tobin *et al.*, 2012; Tobin *et al.*, 2015).

Class 0

In a physical description, Class 0 protostars are surrounded by a massive protostellar envelope constituting at least 50% of the total mass of the protostar-envelope system. Such envelopes have typical sizes of 10^4 AU and might harbour a thick protodisk. The spectral energy distribution of Class 0 sources peaks at submillimeter wavelengths - tracing the presence of cold material in their infalling envelope - and it is characterized by the lack of emission in the near-infrared (Andre *et al.*, 1993; Table 1.2). Typical bolometric temperatures for this class are $\leq$ 70 K (Chen *et al.*, 1995) and the submillimeter-to-bolometric luminosity ratio $L_{\rm submm}/L_{\rm bol}$ is $>$ 0.5 % (Dunham *et al.*, 2014).

The estimated life-time of the Class 0 stage is $\approx$50 000 yrs (Kristensen and Dunham, 2018) and it is characterized by the ejection of material through the launch of outflows and jets sometimes associated with Herbig-Haro objects (Herbig, 1950; Haro, 1952). These are small nebulae typically extending for 20−30″ and detected from peculiar bright clumps of gas located along the outflow direction (Reipurth and Bally, 2001). They are indicators of the powerful mass-loss from newly born stars. Figure 1.3 depicts an example of Herbig-Haro objects within the giant molecular outflow launched by the multi-protostellar system IRAS05417+0907 (Reipurth and Friberg, 2021). How outflows affect the chemical structure of the protostellar envelope and in particular the exact balance of molecules in the gas- and solid-state is one of the topics of Chapters 5, 6, and 7.

Class I

From a physical point of view, Class I protostars also exhibit an envelope - although less massive than the Class 0 one - and they are surrounded by a disk with a radius in the range $\approx$25−500 AU (Williams and Cieza, 2011).

The emission of Class I sources is a composite of the envelope and of the disk contributions. The spectral energy distribution of Class I sources peaks in the mid-/far-infrared (Figure 1.2) and it is characterized by the 9.7 μm absorption band of dust silicates (Henning, 2010; Henning and Meeus, 2011). The spectral index is > 0.3 (Table 1.2) and the bolometric temperature is in the range 650 K < $T_{\rm bol}$ ≤ 2800 K (Chen *et al.*, 1995). The submillimeter-to-bolometric luminosity ratio $L_{\rm submm}/L_{\rm bol}$ is < 0.5 % (Dunham *et al.*, 2014). As for Class 0 sources, also Class I protostars manifest powerful outflows and Herbig-Haro objects, responsible for carving a cavity in Class I envelopes. However, these flows are typically less energetic compared to the earliest class (e.g., Mottram *et al.*, 2017).

The Atacama Large Millimeter/Submillimeter Array (ALMA) and other interferometers, revealed the presence of disks surrounding multiple Class I sources (e.g., Harsono *et al.*, 2014; Artur de la Villarmois *et al.*, 2019) and a number of Class 0 objects (e.g., Tobin *et al.*, 2012; Segura-Cox *et al.*, 2018). Since protoplanetary disks form already at these early stages, the study of Class 0 and I sources provides important clues on the initial physical and chemical conditions for planet formation.

1.2 CHEMICAL PROCESSES IN STAR-FORMING REGIONS

After describing the formation of low-mass stars, and introducing the earliest protostellar stages, the remainder of this chapter will focus on the chemical evolution of the material involved in the star-formation process. Before outlining the changes registered in the composition of the material throughout this journey, the following two sections will provide a summary overview of the chemical processes in star-forming environments. These can be divided into two groups, depending on the state of matter in which they occur: the gas-phase chemistry and the solid-state chemistry. The latter takes place on the dust grain surfaces which are covered with ice mantles, composed by water and other volatile species. These two chemistries are highly intertwined and specific types of reactions take place exclusively in one of the two phases, leading to different products. Since gas-phase molecules can condense on the ice mantles and, in turn, solid-state molecules on the grain surfaces can be released to the gas-phase, the balance between the gas-phase chemistry and the solid-state chemistry is crucial for the chemical evolution of interstellar material. One of the most obvious example of the gas and ice interplay is the methanol-mediated chemistry. Methanol can be produced on the grain surfaces upon hydrogenation of condensed CO molecules (e.g., Watanabe and Kouchi, 2002; Fuchs *et al.*, 2009), and it is involved in the formation of more complex molecules (e.g., Garrod *et al.*, 2008). Consequently, the gas and ice interplay plays a major role in setting the initial chemical conditions for planet formation (van Dishoeck and Bergin, 2020).

1.2.1 *Gas-phase chemistry*

The chemistries of star-forming regions and those of planets differ because these environments are characterized by different physical conditions. Table 1.1 shows that the density of star-forming sites is significantly lower

compared to planetary atmospheres. This inhibits three-body reactions in the gas-phase, i.e., $A + B + C \rightarrow ABC^* \rightarrow AB + C$, which are common on Earth. Additionally, the typical temperatures of bulk material in regions of star and planet formation are far too low for reactions with activation energy barriers to occur (Herbst and Klemperer, 1973; Watson, 1973), except in regions in the vicinity of the newly formed protostar. Consequently, the reactions governing the chemistry of stellar nurseries are exothermic, that is they are barrierless and release energy in the form of heat (Herbst and Klemperer, 1973). The principal gas-phase reaction mechanisms occurring under the physical conditions outlined in Table 1.1 can be divided into three groups (Figure 1.4): bond formation, bond destruction and bond rearrangement.

Bond formation

Among the gas-phase bond formation reactions, the most effective pathway is *radiative association* (Herbst and Klemperer, 1973):

$$A + B \rightarrow AB^* \rightarrow AB + h\nu \tag{1.2}$$

during which the collision of two gas-phase species A and B leads to the formation of an unstable complex AB^*. This complex is stabilized by the formation of a bond between A and B, and through the emission of a photon. Since this mechanism requires gas-phase densities high enough for collisions to manifest, it implies that the principal reactant is the most abundant element in star-forming regions, i.e. atomic or molecular hydrogen (Herbst and Klemperer, 1973).

Bond destruction

The dominating bond destruction channel in regions subjected to UV radiation, e.g., circumstellar environments, photon-dominated regions (PDRs), is *photodissociation* (Hollenbach and Tielens, 1999):

$$AB + h\nu \rightarrow A + B. \tag{1.3}$$

This destruction pathway can be direct, indirect or spontaneous. Most of the interstellar molecules undergo direct photodissociation, where a molecule is excited into a dissociative electronic state upon absorption of a photon. The energy of the incident photon needs to be above the bond dissociation energy for the dissociation to occur.

In the indirect channel, the molecule is excited to a bound electronic state, and then falls into a dissociative state, i.e., *predissociation* (van Dishoeck and Black, 1988; van Dishoeck, 1988). Alternatively, from the bound electronic state, the excited molecule can decay by spontaneously emitting a photon, i.e., *spontaneous radiative association* (van Dishoeck and Black, 1988; Lee *et al.*, 1996). In the absence of UV irradiation, chemical bonds can be destroyed via collisions with electrons and cosmic rays in a process called *dissociative recombination*:

$$AB + e^- \rightarrow A + B. \tag{1.4}$$

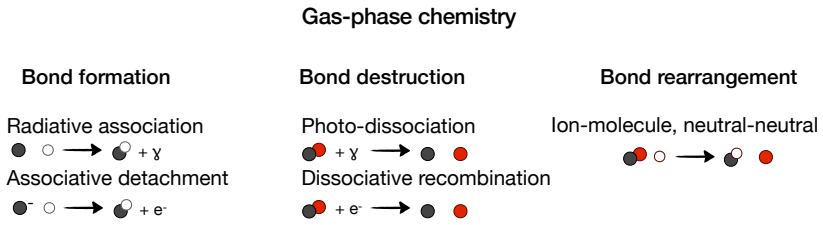

FIGURE 1.4: Schematic representation of the most common gas-phase chemical reactions in star-forming regions. Credit: Öberg and Bergin (2021).

Bond rearrangement

A particularly important group of reactions in the gas-phase of the interstellar medium is the one where the bonds in a molecule are rearranged:

$$AB + C \rightarrow A + BC \tag{1.5}$$

where the reactants are ions and molecules or neutral species only, i.e, *ion-molecule reactions* or *neutral-neutral reactions*. Ion-molecule reactions consists of the ion-capture by a molecule due to the long-range charge attractions between the two reactants, creating an induced dipole moment (Langevin, 1905). These reactions are crucial in gas-phase chemistry and are for example responsible for the formation of the second most abundant molecule in the Universe, CO:

$$C^+ + OH \rightarrow CO^+ + H \tag{1.6}$$

$$CO^+ + H_2 \rightarrow HCO^+ + H \tag{1.7}$$

followed by a dissociative recombination of HCO^+ to form CO + H (van Dishoeck and Black, 1986).

The gas-phase chemistry in dense molecular clouds - especially ion-molecule reactions - is powered by the activity of the simplest polyatomic molecule, protonated molecular hydrogen (H_3^+) (Herbst and Leung, 1989; Dalgarno, 1994; Oka, 2006). H_3^+ is the product of the ionization of H_2 by cosmic-rays or X-rays and its successive protonation (Stecher and Williams, 1969; Stevenson and Schissler, 1958). It is abundantly synthesised in molecular clouds and it has a high chemical reactivity. Being a strong acid, it can donate its "extra" proton to neighboring molecules triggering a large number of ion-molecule reactions.

Neutral-neutral reactions are slower compared to ion-molecule reactions because the reactants are non-charged species and the reactions might have activation energy barriers. Therefore, they typically occur at higher temperatures relative to ion-molecule reactions. For instance, they account for the synthesis of fundamental astrochemical species such as hydroxyl radical (OH) and H_2O in hot gas ($T > 400$ K; e.g., Wagner and Graff, 1987):

$$O + H_2 \rightarrow OH + H \tag{1.8}$$

$$OH + H_2 \rightarrow H_2O + H. \tag{1.9}$$

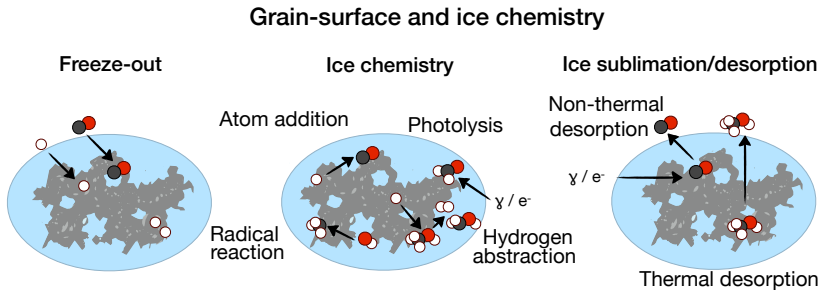

FIGURE 1.5: Schematic representation of the most common grain-surface and ice chemistry reactions in star-forming regions. Credit: Öberg and Bergin (2021).

Recent studies have proved the importance of neutral-neutral reactions not only in high-temperature regions, e.g., hot cores. For instance, it has been shown that they play a key role in the formation of organic molecules akin methoxy (CH_3O), dimethyl ether (CH_3OCH_3) and methyl formate ($HCOOCH_3$) in cold gas (Balucani *et al.*, 2015). This particular synthesis is a good example of interplay between gas and ice chemistry. In fact, the chain of neutral-neutral reactions leading to the three molecules initiates upon the release of methanol from the ice mantles (see Sect. 1.2.2).

The efficiency of complex molecule formation via gas-phase pathways compared to solid-state chemistry reactions is not well constrained at present (Sect. 1.2.2). Currently, quantum chemistry models are exploring a number of feasible chemical routes in cold regions. The reactants are typically methanol (Shannon *et al.*, 2013; Antiñolo *et al.*, 2016) or ethanol (CH_3CH_2OH; Skouteris *et al.*, 2018). The increasing detections of prebiotic molecule precursors are motivating the need for computational studies on the formation and reactivity of such large molecules in the gas phase (e.g., Redondo *et al.*, 2017a; Redondo *et al.*, 2017b).

1.2.2 *Grain-surface and ice chemistry*

The presence of dust grains transforms the chemistry of star-forming environments, expanding the types of chemical processes available and enhancing chemical complexity (Figure 1.5). In fact, although dust grains represent a minor fraction of the total mass of stellar nurseries ($\approx$ 1%; Sect. 1.1), their role as catalysts has a profound impact on the overall interstellar chemistry (Hasegawa *et al.*, 1992; Hasegawa and Herbst, 1993).

In the coldest regions of dense clouds ($T \approx 10$ K) gas-phase species colliding with the surfaces of dust grains are adsorbed in a process called *freeze-out*. This occurs to most interstellar species except for He and H_2, which sublimate at these low temperatures (Hollenbach and Salpeter, 1971). Freeze-out is responsible for the build-up of layers onto the grain surfaces, commonly referred to as ice mantles (Pickles and Williams, 1977; Hasegawa *et al.*, 1992; Ruffle and Herbst, 2001a). Molecules and atoms accreting onto ice mantles, i.e., adsorbates, are either chemically bounded to the surface of the grain, i.e., *chemisorption*, or adsorbed via van der Waals forces, i.e., *physisorption*. Van der Waals forces are weaker compared to molecular bonds implying that physisorbed species require less energy to be released to the gas-phase with respect to chemisorbed species, e.g., Buch and Czerminski

(1991), Bolina and Brown (2005), and Shimonishi *et al.* (2018).

In general, surface reactions are believed to proceed via one of the following mechanisms: *Langmuir-Hinshelwood*, *Eley-Rideal* and *Kasemo-Harris* also referred to as *hot atom*. In the Langmuir-Hinshelwood mechanism, both reactants are mobile and diffuse between binding sites on the grain surface either by tunneling across the potential energy barrier or via thermal hopping until they meet and react (Langmuir, 1922; Hinshelwood, 1940). Alternatively, in the *Eley-Rideal* mechanism, the gas-phase species reacts with a stationary adsorbate (Eley and Rideal, 1940). Finally, in the hot atom mechanism, a gas-phase species collides with the grain and has sufficient kinetic energy to move on the surface until it encounters an adsorbate to react with (Harris and Kasemo, 1981). Among the three mechanisms the Langmuir-Hinshelwood is the most studied and included in astrochemical models (Kolasinski, 2002), whereas the hot atom pathway is thought not to prevail as the hot atom is typically thermalized before encountering a reactant (Cuppen *et al.*, 2017).

The molecules residing onto ice layers can undergo the set of reactions illustrated in Figure 1.5. One of the dominant reactions is H atom addition, i.e. *hydrogenation*, as H atoms due to their small sizes diffuse on grain surfaces via tunneling (Hasegawa *et al.*, 1992). Atom addition reactions lead to the formation of H_2, the most abundant molecule in space (Gould and Salpeter, 1963; Hollenbach and Salpeter, 1971; Watson and Salpeter, 1972; Wakelam *et al.*, 2017). When H atoms react sequentially with heavier elements such as oxygen atoms or O_2 and O_3, the most abundant ice species is formed, H_2O (Tielens and Hagen, 1982; Cuppen and Herbst, 2007; Ioppolo *et al.*, 2008; Miyauchi *et al.*, 2008). This process involves a number of reactions in which H atoms are added and abstracted. Similarly, H atom additions produce ammonia (NH_3) and methane (CH_4) onto ice mantles (van de Hulst, 1946; Fedoseev *et al.*, 2015b; Qasim *et al.*, 2020). When CO freezes out, a number of chemical routes open up. Most importantly, carbon dioxide (CO_2) is produced (Ruffle and Herbst, 2001b; Ioppolo *et al.*, 2011) and simultaneously, the sequential hydrogenation of CO initiates the formation of complex organic molecules (COMs) such as methanol (Charnley *et al.*, 1997; Watanabe and Kouchi, 2002; Fuchs *et al.*, 2009):

$$\mathrm{CO} \longrightarrow \mathrm{HCO^{\bullet}} \longrightarrow \mathrm{H_2CO} \longrightarrow \mathrm{CH_3O^{\bullet}/^{\bullet}CH_2OH} \longrightarrow \mathrm{CH_3OH} \qquad (1.10)$$

where the pathway via $CH_3O^{\bullet}$ is the energetically favourable one, and hence, the prevalent (Song and Kästner, 2017; Simons *et al.*, 2020). The implications of the formation of CH_3OH in star-forming regions will be discussed in Sect. 1.4.

In general, the reactions leading to complex molecules involve, besides atoms and molecules, radicals (e.g., Garrod *et al.*, 2008; Öberg *et al.*, 2009b; Chuang *et al.*, 2017), as can be seen in the reaction above. Radicals are typically produced during H addition and abstraction reactions or via photolysis and dissociative recombination. Most importantly, energetic processing is thought to be the most dominant source of radicals via photochemistry and radiation chemistry (Arumainayagam *et al.*, 2019). Reactions involving radical additions are considered fundamental to explain the high abundances

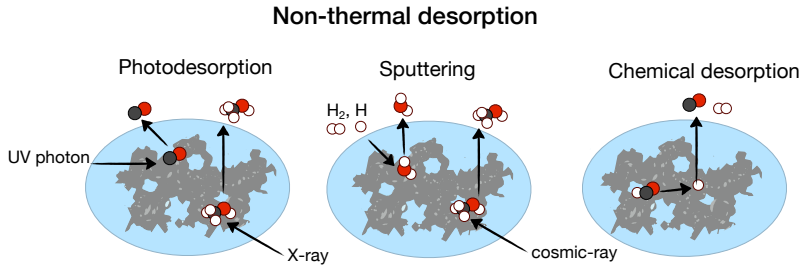

FIGURE 1.6: Schematic representation of the most common non-thermal desorption mechanisms in star-forming regions. Adapted from Öberg and Bergin (2021).

of complex molecules in embedded young protostars (Garrod *et al.*, 2008; see Sect. 1.3).

1.2.3 *Desorption processes*

Molecules and atoms residing onto ice mantles can be released to the gas-phase through *desorption* reactions (Figure 1.5). These, jointly with the freeze-out process, govern the interplay between solid-state and gas-phase in star-forming regions, enhancing the chemical complexity of protostars. Desorption reactions are grouped into two categories: thermal and non-thermal.

Thermal desorption

Thermal desorption is triggered upon global heating of the grain which leads to the sublimation of the ice mantles. This chemical process occurs when the dust temperature is higher than the sublimation temperature of a chemical species. It is the most studied desorption reaction, both theoretically (e.g., Penteado *et al.*, 2017; Das *et al.*, 2018; Ferrero *et al.*, 2020) and experimentally, through temperature programmed desorption (TPD) experiments (e.g., Fraser *et al.*, 2001; Collings *et al.*, 2004; Öberg *et al.*, 2005; Bisschop *et al.*, 2006). TPD experiments revealed that thermal desorption is more complex than initially thought as it is sensitive to multiple parameters, most importantly the ice morphology and composition (e.g., Fayolle *et al.*, 2016). Thermal desorption reactions are particularly crucial in protoplanetary disks, because the radii at which they occur determine the so-called *snowlines* (or icelines) which have important consequences on the chemical composition of forming planets (Öberg *et al.*, 2011b; Eistrup *et al.*, 2016; van 't Hoff *et al.*, 2017; Grassi *et al.*, 2020).

Non-thermal desorption

Non-thermal desorption is a consequence of local heating of the grain, followed by a partial sublimation of the ice mantles (Figure 1.6). The factors leading to non-thermal desorption processes are several and they are thought to occur in the cold regions of protostellar envelopes. For instance, the most investigated one is *photodesorption*, when the local heating is caused by impinging UV photons on the grain surface (Westley *et al.*, 1995; Öberg *et al.*, 2009a; Öberg *et al.*, 2009b; Fayolle *et al.*, 2011). This process is not as straightforward because it can lead to the photodissociation of the interested species, a channel that has been explored with molecular

dynamics simulations (Andersson *et al.*, 2006; Andersson and van Dishoeck, 2008), and in the laboratory (e.g., Bertin *et al.*, 2016; Cruz-Diaz *et al.*, 2016; Martín-Doménech *et al.*, 2016) especially for H_2O and CH_3OH.

Non-thermal desorption can also be triggered by *sputtering* when atoms and neutral species collide with the grain surfaces and have sufficient kinetic energy to eject ice molecules into the gas-phase. This is considered as the dominant non-thermal desorption process in shocked regions (e.g., Jørgensen *et al.*, 2004; Jiménez-Serra *et al.*, 2008; Kristensen *et al.*, 2010; Suutarinen *et al.*, 2014; Allen *et al.*, 2020). *Cosmic-ray induced sputtering* is also a viable route, and the efficiency of this process has been constrained in the laboratory for pure H_2O, CO_2:CH_3OH and H_2O:CH_3OH:CH_3COOCH_3 ice analogues (Dartois *et al.*, 2018; Dartois *et al.*, 2019; Dartois *et al.*, 2020). These experiments demonstrated that, compared to photodesorption, a large fraction of species is non-thermally desorbed intact during sputtering by cosmic rays.

More recently, an additional non-thermal desorption mechanisms has been proposed in the literature to explain the abundance of complex organics in UV-shielded and quiescent regions (Garrod *et al.*, 2007). It is referred to as *chemical desorption* or *reactive desorption* (Dulieu *et al.*, 2013; Vasyunin and Herbst, 2013; Minissale *et al.*, 2016b; Cazaux *et al.*, 2016; Vasyunin *et al.*, 2017). The factor triggering this desorption channel is the exothermicity of a reaction taking place on the grain surfaces, which is able to expel the product of the reaction or the neighbouring species. Finally, a novel mechanism has been tested called *X-ray photodesorption*. This process is thought to have an impact on the desorption of ice mantles in protoplanetary disks initiated by X-rays emitted from the central protostar (Andrade *et al.*, 2010; Dupuy *et al.*, 2018; Jiménez-Escobar *et al.*, 2018; Ciaravella *et al.*, 2020; Basalgète *et al.*, 2021a; Basalgète *et al.*, 2021b).

This discussion clearly shows that desorption processes, especially the non-thermal ones, are far from being well understood. Laboratory data exists only for a discrete number of species and many of the above mechanisms are not yet included into astrochemical models. In addition to this, it is a challenging task to distinguish between the various non-thermal desorption mechanisms from an observational point of view. This implies that numerous venues exists for future studies on this topic.

After describing the physical processes during star-formation (Sect. 1.1) and the chemical processes involved in it (Sect. 1.2), the upcoming section "brings together the two worlds" by outlining which type of chemistry and molecular complexity is observed around protostars.

1.3 THE GAS AND ICE INTERPLAY IN PROTOSTELLAR ENVELOPES

The gas and ice interplay is ubiquitous in the Universe, and it is involved in all the stages of star and planetary system formation. It is responsible for changes in the ice and gas composition of the envelope material incorporated into protoplanetary disks and, eventually, planet-forming zones (Öberg and Bergin, 2021; van Dishoeck and Bergin, 2020). In this context, a major unanswered question in astrochemistry is whether the disk material and the proto-planets preserve the chemical fingerprints of the parental molecular

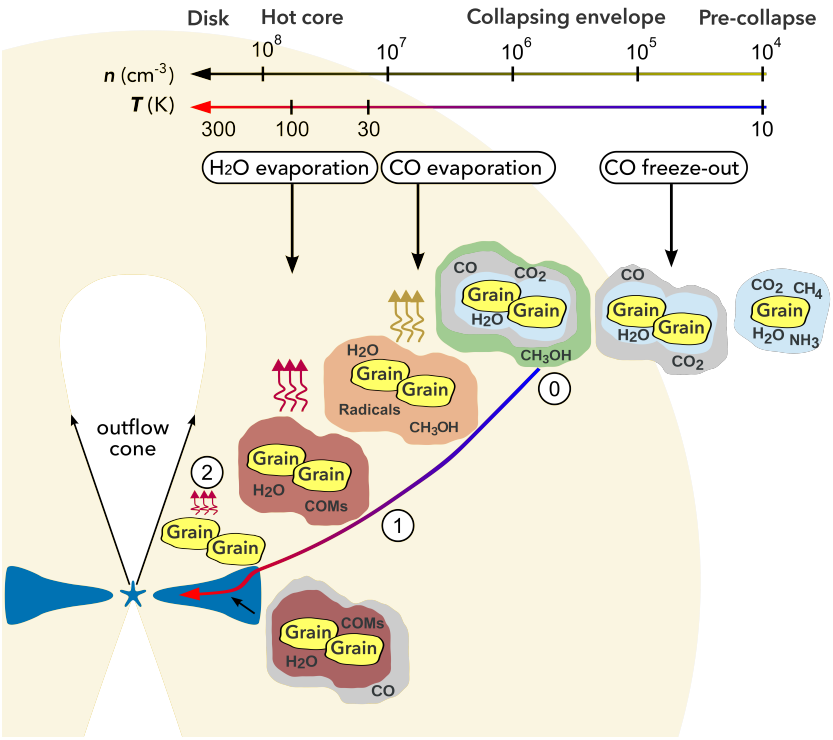

FIGURE 1.7: Illustration of the chemical evolution of the material during the formation of a low-mass star, from the pre-stellar core to the protoplanetary disk. The material experiences an increase in chemical complexity in the protostellar envelope. The numbers 0, 1, and 2 refer to the formation of the 0th-, 1st-, and 2nd-generation of organic molecules on the ice mantles. The grains are not to scale and the acronym COMs stands for Complex Organic Molecules (COMs). Adapted figures from Herbst and van Dishoeck (2009) and Boogert *et al.* (2015).

cloud, i.e., *inheritance* scenario, or not, due to various degrees of thermal processing, i.e., *reset* scenario (Pontoppidan and Blevins, 2014). At present, neither of the two hypotheses can be discarded, as the material of pristine Solar System objects, e.g., comets, share similarities with the protostellar material (Drozdovskaya *et al.*, 2019). In contrast, the organic matter found in carbonaceous chondrites is often aqueously altered and has a more complex chemical structure (Alexander *et al.*, 2007).

The composition of the protostellar material varies according to its location in the collapsing envelope, and by consequence, on the underlying chemistry (Figure 1.7). This thesis focuses on the chemistry occurring in the outer regions of the envelope ($\approx 10^4$ AU), characterized by low temperatures ($\approx 10-20$ K). The prevalent process under these physical conditions is freeze-out, which leads to the built up of ice layers (see Sect. 1.2.2). The gas-species accreting onto the ice grains (e.g., CO) undergo atom addition/abstraction reactions producing simple molecules (e.g., H_2O, CO_2) and larger organic molecules, e.g. CH_3OH, CH_3CH_2OH sometimes referred to as 0th-generation species (Charnley, 1997). Non-thermal desorption processes prevail during this cold phase (Figure 1.6).

As the material falls inward towards the forming protostar, it warms up. The increase in temperature impacts considerably the ice chemistry compared to the gas-phase chemistry (Herbst and van Dishoeck, 2009). Volatile molecules such as CO, N_2, and CH_4 start to thermally desorb from

the ice mantles when the dust temperature is ~20 K (Collings *et al.*, 2004; Bisschop *et al.*, 2006; Acharyya *et al.*, 2007). Concurrently, less volatile species remain on the ice mantles and become more mobile, but yet too stable to start a rich chemistry. The ice chemistry during the warm-up phase is thought to be dominated by radical-radical addition surface reactions (e.g., $HCO^{\bullet}$ + $CH_3O^{\bullet}$) triggered by a cosmic-ray induced photochemistry (Garrod and Herbst, 2006; Garrod *et al.*, 2008). The radicals are produced during the photo-dissociation of 0^{th}-generation species. The products of the warm-up chemistry are denoted as 1^{st}-generation species. Some examples are saturated species such as formic acid (HCOOH) and methyl formate.

When the material reaches the innermost regions of the envelope (< 200 AU; Schöier *et al.*, 2002), the temperatures are above 100 K. Under these conditions, all the ice mantles are thermally desorbed, and by consequence, chemical reactions uniquely take place in the gas (Figure 1.4). This phase, referred to as *hot-corino*, is characterized by a rich-chemistry as the high temperatures (100−300 K) permit the occurrence of endothermic reactions (i.e., routes requiring energy to overcome the potential energy barrier between reactants and products). Ion-molecule and neutral-neutral reactions produce larger complex organic molecules known as 2^{nd}-generation species. Examples of this class of molecules include formamide (NH_2CHO) and ethylene glycol ($HOCH_2CH_2OH$; Jørgensen *et al.*, 2016).

A fraction of the molecules produced in hot-corinos is inevitably photo-dissociated because they are subjected to the irradiation from the protostar. However, there is some evidence that part of the envelope material can be incorporated into the protoplanetary disk, and hence inherited to the planet and comets forming zones. This is suggested by numerical models by e.g., Visser *et al.* (2009) and Visser *et al.* (2011) which revealed that some of the disk material is heavily processed, whereas some remains pristine. From an observational point of view, Drozdovskaya *et al.* (2019) found a correlation between the relative abundances of CHO-, N-, and S-bearing molecules detected towards the protostellar system IRAS 16293-2422 and the comet 67P/Churyumov-Gerasimenko. This indicates a certain degree of inheritance from the protostellar stages to the locations in the disk where planets and comets are formed. Recent laboratory experiments successfully synthesized glycine, the simplest amino acid, through atom and radical-radical addition, without the need for energetic processing (Ioppolo *et al.*, 2021). This implies that molecules as complex as glycine can plausibly form at much earlier stages in the star-formation process than previously thought, e.g., during the cold phase or earlier. This result and the unambiguous detection of glycine in cometary material (Altwegg *et al.*, 2016) suggest that the coldest regions of disk mid-planes might be favourable for the conservation of material inherited from the molecular cloud or for the production of molecules biologically relevant for life.

The last section of this introduction presents the principal molecule studied in this thesis, methanol (CH_3OH), with a particular focus on the astrochemical implications concerning its presence in star-forming regions.

1.4 THE ASTROCHEMICAL RELEVANCE OF METHANOL

Methanol (or methyl alcohol) is the simplest and most abundant complex organic molecule and it is ubiquitous in stellar nurseries. Its presence has been inferred in the gas-phase of pre-stellar cores (e.g., Bizzocchi *et al.*, 2014), starless cores (e.g., Spezzano *et al.*, 2020) hot-cores and hot-corinos (e.g., Jørgensen *et al.*, 2020), protoplanetary disks (Walsh *et al.*, 2016; van 't Hoff *et al.*, 2018) and cometary material (e.g., Hoban *et al.*, 1993; Bockelee-Morvan *et al.*, 1994; Mumma and Charnley, 2011; Le Roy *et al.*, 2015; Rubin *et al.*, 2019). Its solid-state counterpart has also been detected towards a variety of astrophysical environments, for instance in the ice mantles of low- and high-mass protostars (Boogert *et al.*, 2015), pre-stellar and starless cores (Chu *et al.*, 2020; Goto *et al.*, 2020), on the icy surface of the Kuiper belt object Arrokoth (Grundy *et al.*, 2020), and in the Murchison CM2 chondrite (Jungclaus *et al.*, 1976).

Extensive laboratory studies on CH_3OH formation in pre-stellar and protostellar environments have been carried out in the past decades. At higher cloud extinctions ($A_V > 9$) and low temperatures, once the catastrophic CO freeze-out has occurred (Boogert *et al.*, 2011; Chiar *et al.*, 2011), the formation of methanol is dominated by the CO + H reaction (Sect. 1.2.2). This chemical pathway is considered the most relevant source of CH_3OH in star-forming regions (e.g., Watanabe and Kouchi, 2002; Fuchs *et al.*, 2009). An important route to account for the presence of CH_3OH at earlier stages, prior to the heavy CO freeze-out, has been studied experimentally by Qasim *et al.* (2018). At a cloud visual extinction (A_V) of ≈ 3 mag, only a low fraction of gas-phase CO accreates onto the dust grains, due to low gas densities at this extinction (Pontoppidan, 2006). Therefore, the grain surfaces are mostly composed by H_2O-rich ices that contain CH_4, but CH_3OH can nevertheless form via the sequential surface reaction chain (Qasim *et al.*, 2018):

$$CH_4 + {}^{\bullet}OH \longrightarrow {}^{\bullet}CH_3 + H_2O \tag{1.11}$$

where the hydroxyl radical mediates the H abstraction. This is followed by the recombination of the two radicals:

$${}^{\bullet}CH_3 + {}^{\bullet}OH \longrightarrow CH_3OH. \tag{1.12}$$

Apart from being omnipresent in interstellar and circumstellar environments, methanol is regarded as the gateway species for the formation of complex organic molecules in the ISM (Öberg *et al.*, 2009b; Herbst and van Dishoeck, 2009). The experiments by Fedoseev *et al.* (2015a) and Chuang *et al.* (2016) reveal that CH_3OH is plausibly a key reactant in the production of complex organics in the cold phase of the star-formation process (Figure 1.7). These studies show that the radicals originating from CH_3OH, i.e., ${}^{\bullet}CH_3$ and ${}^{\bullet}OH$, are able to combine with other species present on the ice analogs, leading to the production of larger organics akin glycerol ($HOCH_2CH(OH)CH_2OH$), an important component of cell membranes (Fedoseev *et al.*, 2017). These chemical routes occur via non-energetic processing, i.e., under low temperatures ($T < 20$ K) and in the absence of UV radiation.

Simultaneously, the production of complex organics from CH_3OH has been studied in the laboratory via energetic processing (cosmic ray-, UV-induced). It has been seen that cosmic ion irradiation of methanol can lead to the production of complex organics (e.g., methyl formate; Modica *et al.*, 2012). Additionally, figure 1.8 displays the chemical network triggered upon UV-irradiation of CH_3OH-containing ice analogs (e.g., pure CH_3OH, pure CO and CH_4:CH_3OH ices). The products are a suite of more complex organic species such as ethanol (CH_3CH_2OH), dimethyl ether (CH_3OCH_3) and glycolaldehyde ($HOCH_2CHO$) (e.g., Bennett *et al.*, 2007; Öberg *et al.*, 2009b). These experiments suggest that the formation of methanol is fundamental for the development of molecular complexity in UV-irradiated regions, during the protostellar stage.

The hypothesis above is supported further by UV-irradiation experiments of ice mixtures of different compositions such H_2O:CH_3OH by Meinert *et al.* (2016) and Nuevo *et al.* (2018). These studies have synthesized, among several compounds of biological interests, ribose (Meinert *et al.*, 2016) and 2-deoxyribose, the sugar composing the deoxyribonucleic acid (DNA) (Nuevo *et al.*, 2018). Continuous advances in laboratory experiments (via energetic and non-energetic processing) and models will help accounting for the role of methanol in the ISM and for the molecular complexity observed (e.g., Jiménez-Serra *et al.*, 2020) - and yet to be observed in star-forming regions, and ultimately to link it to the origin of life on Earth.

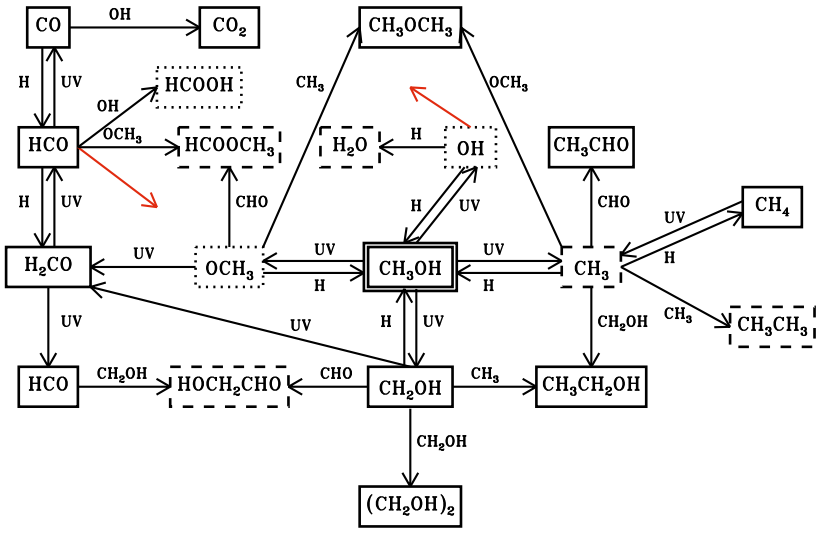

FIGURE 1.8: The CH_3OH reaction network upon UV-irradiation of pure CH_3OH ice (solid boxes), pure CO ice and CH_4:CH_3OH ice analogs (dashed boxes). Credit: Öberg *et al.* (2009b).

The main aim of this thesis is to study the interplay between methanol gas and ice through millimetric and infrared observations of solar-type protostellar envelopes. In particular, to access the dependencies of the methanol gas-to-ice ratio on different physical conditions. This is achieved by obtaining and comparing direct measurements of gas-phase and ice methanol towards protostars located in the three nearby star-forming regions presented in Chapter 3.

Bibliography

1. ALMA Partnership *et al.*, *ApJ* **808**, L3 (2015).
2. K. Acharyya *et al.*, *A&A* **466**, 1005–1012 (2007).
3. C. M. O. D. Alexander *et al.*, *Geochim. Cosmochim. Acta* **71**, 4380–4403 (2007).
4. V. Allen, M. Cordiner, S. Charnley, *arXiv e-prints* (2020).
5. K. Altwegg *et al.*, *Science Advances* **2**, e1600285–e1600285 (2016).
6. F. O. Alves *et al.*, *ApJ* **904**, L6 (2020).
7. J. Alves, M. Lombardi, C. J. Lada, *A&A* **565**, A18 (2014).
8. S. Andersson, E. F. van Dishoeck, *A&A* **491**, 907–916 (2008).
9. S. Andersson *et al.*, *J. Chem. Phys.* **124**, 064715–064715 (2006).
10. D. P. P. Andrade, M. L. M. Rocco, H. M. Boechat-Roberty, *MNRAS* **409**, 1289–1296 (2010).
11. P. André *et al.*, in *Protostars and Planets VI* (Beuther, Henrik et al., 2014), p. 27.
12. P. André *et al.*, *A&A* **518**, L102 (2010).
13. P. André, *Comptes Rendus Geoscience* **349**, 187–197 (2017).
14. P. Andre, D. Ward-Thompson, M. Barsony, *ApJ* **406**, 122 (1993).
15. S. M. Andrews *et al.*, *ApJ* **869**, L41 (2018).
16. M. Ansdell *et al.*, *AJ* **160**, 248 (Dec. 2020).
17. M. Antiñolo *et al.*, *ApJ* **823**, 25 (2016).
18. E. Artur de la Villarmois *et al.*, *A&A* **626**, A71 (2019).
19. C. R. Arumainayagam *et al.*, *Chemical Society Reviews* **48**, 2293–2314 (2019).
20. Y. Aso *et al.*, *ApJ* **863**, 19 (2018).
21. R. Bachiller *et al.*, *A&A* **295**, L51 (1995).
22. R. Bachiller *et al.*, *A&A* **335**, 266–276 (1998).
23. J. Bally, in *Handbook of Star Forming Regions, Volume I* (Reipurth, B., 2008), vol. 4, p. 459.
24. N. Balucani, C. Ceccarelli, V. Taquet, *MNRAS* **449**, L16–L20 (2015).
25. P. J. Barnes *et al.*, *ApJ* **812**, 6 (2015).
26. D. Barrado *et al.*, *A&A* **526**, A21 (2011).
27. D. Barrado *et al.*, *A&A* **612**, A79 (2018).
28. R. Basalgète *et al.*, *A&A* **647**, A35 (2021).
29. R. Basalgète *et al.*, *A&A* **647**, A36 (2021).
30. M. R. Bate, *MNRAS* **475**, 5618–5658 (2018).
31. A. Bayo *et al.*, *A&A* **536**, A63 (2011).
32. C. P. M. Bell *et al.*, *MNRAS* **434**, 806–831 (2013).
33. C. J. Bennett *et al.*, *ApJ* **660**, 1588–1608 (2007).
34. P. J. Benson, P. C. Myers, *ApJS* **71**, 89 (1989).
35. E. A. Bergin, M. Tafalla, *ARA&A* **45**, 339–396 (2007).
36. J. B. Bergner *et al.*, *ApJ* **841**, 120 (2017).
37. J. B. Bergner *et al.*, *ACS Earth and Space Chemistry* **3**, 1564–1575 (2019).
38. M. Bertin *et al.*, *ApJ* **817**, L12 (2016).
39. E. A. Bibo, P. S. The, D. N. Dawanas, *A&A* **260**, 293–302 (1992).
40. S. E. Bisschop *et al.*, *A&A* **449**, 1297–1309 (2006).
41. L. Bizzocchi *et al.*, *A&A* **569**, A27 (2014).

42. P. Bjerkeli *et al.*, *A&A* **546**, A29 (2012).
43. P. Bjerkeli *et al.*, *A&A* **595**, A39 (2016).
44. R. D. Blandford, D. G. Payne, *MNRAS* **199**, 883–903 (1982).
45. S Blanksby, G Ellison, *Accounts of Chemical Research* **36**, 255–263 (2003).
46. J. Blum, G. Wurm, *ARA&A* **46**, 21–56 (2008).
47. D. Bockelee-Morvan *et al.*, *A&A* **287**, 647–665 (1994).
48. C. F. Bohren, D. R. Huffman, *Absorption and scattering of light by small particles* (New York: Wiley, 1983).
49. A. S. Bolina, W. A. Brown, *Surface Science* **598**, 45–56 (2005).
50. W. B. Bonnor, *ZAp* **39**, 143 (1956).
51. S. Bontemps *et al.*, *A&A* **518**, L85 (2010).
52. A. C. A. Boogert, P. A. Gerakines, D. C. B. Whittet, *ARA&A* **53**, 541–581 (2015).
53. A. C. A. Boogert *et al.*, *A&A* **360**, 683–698 (2000).
54. A. C. A. Boogert *et al.*, *ApJ* **678**, 985–1004 (2008).
55. A. C. A. Boogert *et al.*, *ApJ* **729**, 92 (2011).
56. A. C. A. Boogert *et al.*, *ApJ* **777**, 73 (2013).
57. S. Bottinelli *et al.*, *ApJ* **718**, 1100–1117 (2010).
58. F. Brauer, T. Henning, C. P. Dullemond, *A&A* **487**, L1–L4 (2008).
59. D. Bresnahan *et al.*, *A&A* **615**, A125 (2018).
60. D. S. Briggs, F. R. Schwab, R. A. Sramek, in *Synthesis Imaging in Radio Astronomy II* (Taylor, G. B., Carilli, C. L., and Perley, R. A., 1999), vol. 180, p. 127.
61. T. Y. Brooke, K. Sellgren, T. R. Geballe, *ApJ* **517**, 883–900 (1999).
62. A. Brown, *ApJ* **322**, L31 (1987).
63. V. Buch, R. Czerminski, *J. Chem. Phys.* **95**, 6026–6038 (1991).
64. J. V. Buckle *et al.*, *MNRAS* **399**, 1026–1043 (2009).
65. J. V. Buckle *et al.*, *MNRAS* **422**, 521–541 (2012).
66. J. A. Caballero, *A&A* **478**, 667–674 (2008).
67. H. Calcutt *et al.*, *A&A* **616**, A90 (2018).
68. L. Cambrésy, *A&A* **345**, 965–976 (1999).
69. J. A. Cardelli, G. C. Clayton, J. S. Mathis, *ApJ* **345**, 245 (1989).
70. P. Carlhoff *et al.*, *A&A* **560**, A24 (2013).
71. J. M. Carpenter, *AJ* **120**, 3139–3161 (2000).
72. M. M. Casali, C. Eiroa, W. D. Duncan, *A&A* **275**, 195–200 (1993).
73. S. Cazaux *et al.*, *ApJ* **593**, L51–L55 (2003).
74. S. Cazaux *et al.*, *A&A* **585**, A55 (2016).
75. S. Cazaux *et al.*, *ApJ* **849**, 80 (2017).
76. P. Cazzoletti *et al.*, *A&A* **626**, A11 (2019).
77. C. J. Chandler, J. E. Carlstrom, *ApJ* **466**, 338 (1996).
78. N. L. Chapman *et al.*, *ApJ* **690**, 496–511 (2009).
79. S. B. Charnley, A. G. G. M. Tielens, S. D. Rodgers, *ApJ* **482**, L203–L206 (1997).
80. S. B. Charnley, in *IAU Colloq. 161: Astronomical and Biochemical Origins and the Search for Life in the Universe* (Batalli Cosmovici, Cristiano, Bowyer, Stuart, and Werthimer, Dan, 1997), p. 89.
81. H. Chen *et al.*, *ApJ* **445**, 377 (1995).
82. X. Chen, H. G. Arce, *ApJ* **720**, L169–L173 (2010).
83. J. E. Chiar *et al.*, *ApJ* **426**, 240 (1994).
84. J. E. Chiar *et al.*, *ApJ* **570**, 198–209 (2002).
85. J. E. Chiar *et al.*, *ApJ* **731**, 9 (2011).

86. M. Choi, *ApJ* **705**, 1730–1734 (2009).
87. L. E. U. Chu, K. Hodapp, A. Boogert, *ApJ* **904**, 86 (2020).
88. K. J. Chuang *et al.*, *MNRAS* **455**, 1702–1712 (2016).
89. K. J. Chuang *et al.*, *MNRAS* **467**, 2552–2565 (2017).
90. A. Ciaravella *et al.*, *Proceedings of the National Academy of Science* **117**, 16149–16153 (2020).
91. M. P. Collings *et al.*, *ApJ* **583**, 1058–1062 (2003).
92. M. P. Collings *et al.*, *MNRAS* **354**, 1133–1140 (2004).
93. M. S. Connelley, B. Reipurth, A. T. Tokunaga, *AJ* **135**, 2496–2525 (2008).
94. P. S. Conti, E. M. Leep, *ApJ* **193**, 113–124 (1974).
95. A. M. Craigon, http://digitool.lib.strath.ac.uk/R/?func=dbin-jump-full&object_id=27550, PhD thesis, Dept. of Physics, Univ. of Strathclyde, 2015.
96. G. A. Cruz-Diaz *et al.*, *A&A* **592**, A68 (2016).
97. H. M. Cuppen, E. Herbst, *ApJ* **668**, 294–309 (2007).
98. H. M. Cuppen *et al.*, *MNRAS* **417**, 2809–2816 (2011).
99. H. M. Cuppen *et al.*, *Space Sci. Rev.* **212**, 1–58 (2017).
100. A. Dalgarno, in, ed. by B. Bederson, A. Dalgarno (Academic Press, 1994), vol. 32, pp. 57–68.
101. T. M. Dame, P. Thaddeus, *ApJ* **297**, 751–765 (1985).
102. T. M. Dame *et al.*, *ApJ* **322**, 706 (1987).
103. E. Dartois *et al.*, *A&A* **618**, A173 (2018).
104. E. Dartois *et al.*, *Astronomy and Astrophysics* **627**, A55 (2019).
105. E. Dartois *et al.*, *A&A* **634**, A103 (2020).
106. A. Das *et al.*, *ApJS* **237**, 9 (2018).
107. C. J. Davis *et al.*, *MNRAS* **309**, 141–152 (1999).
108. A. Dawes, N. J. Mason, H. J. Fraser, *Phys. Chem. Chem. Phys.* **18**, 1245–1257 (2 2016).
109. C. H. De Vries, G. Narayanan, R. L. Snell, *ApJ* **577**, 798–825 (2002).
110. J. T. Dempsey *et al.*, *MNRAS* **430**, 2534–2544 (2013).
111. J. P. Devlin, *J. Chem. Phys* **96**, 6185–6188 (1992).
112. J. Di Francesco *et al.*, *ApJS* **175**, 277–295 (2008).
113. S. Dib, T. Henning, *A&A* **629**, A135 (2019).
114. O. Dionatos *et al.*, *A&A* **558**, A88 (2013).
115. O. Dionatos *et al.*, *A&A* **563**, A28 (2014).
116. C. J. Dolan, R. D. Mathieu, *AJ* **118**, 2409–2423 (1999).
117. C. J. Dolan, R. D. Mathieu, *AJ* **123**, 387–403 (2002).
118. B. T. Draine, *ARA&A* **41**, 241–289 (2003).
119. B. T. Draine, F. Bertoldi, *ApJ* **468**, 269 (1996).
120. M. N. Drozdovskaya *et al.*, *MNRAS* **490**, 50–79 (2019).
121. A. Duarte-Cabral *et al.*, *A&A* **519**, A27 (2010).
122. F. Dulieu *et al.*, *Scientific Reports* **3**, 1338 (2013).
123. M. M. Dunham *et al.*, in *Protostars and Planets VI* (Beuther, Henrik et al., 2014), p. 195.
124. M. M. Dunham *et al.*, *ApJS* **220**, 11 (2015).
125. R. Dupuy *et al.*, *Nature Astronomy* **2**, 796–801 (2018).
126. A. Duquennoy, M. Mayor, *A&A* **500**, 337–376 (1991).
127. R. Ebert, *ZAp* **37**, 217 (1955).
128. P. Ehrenfreund, S. B. Charnley, *ARA&A* **38**, 427–483 (2000).
129. C. Eiroa, M. M. Casali, *A&A* **223**, L17–L19 (1989).

130. C. Eiroa, A. A. Djupvik, M. M. Casali, in *Handbook of Star Forming Regions, Volume II: The Southern Sky ASP Monograph Publications* (Reipurth, B. ed, 2008), vol. 5, p. 693.
131. C. Eistrup, C. Walsh, E. F. van Dishoeck, *A&A* **595**, A83 (2016).
132. D. D. Eley, E. K. Rideal, *Nature* **146**, 401–402 (1940).
133. I. Evans Neal J. *et al.*, *ApJS* **181**, 321–350 (2009).
134. N. J. Evans II *et al.*, *VizieR Online Data Catalog* **2332** (2014).
135. E. C. Fayolle *et al.*, *ApJ* **739**, L36 (2011).
136. E. C. Fayolle *et al.*, *ApJ* **816**, L28 (2016).
137. G. G. Fazio *et al.*, *ApJS* **154**, 10–17 (2004).
138. G. Fedoseev *et al.*, *MNRAS* **448**, 1288–1297 (2015).
139. G. Fedoseev *et al.*, *MNRAS* **446**, 439–448 (2015).
140. G. Fedoseev *et al.*, *ApJ* **842**, 52 (2017).
141. S. Ferrero *et al.*, *ApJ* **904**, 11 (2020).
142. J. Forbrich, T. Preibisch, *A&A* **475**, 959–972 (2007).
143. J. Forbrich *et al.*, *A&A* **464**, 1003–1013 (2007).
144. D. Foreman-Mackey *et al.*, *PASP* **125**, 306 (2013).
145. H. J. Fraser, E. F. van Dishoeck, *Advances in Space Research* **33**, 14–22 (2004).
146. H. J. Fraser *et al.*, *MNRAS* **327**, 1165–1172 (2001).
147. H. J. Fraser *et al.*, *MNRAS* **353**, 59–68 (2004).
148. S. Frimann, J. K. Jørgensen, T. Haugbølle, *A&A* **587**, A59 (2016).
149. G. W. Fuchs *et al.*, *A&A* **505**, 629–639 (2009).
150. P. A. B. Galli *et al.*, *A&A* **634**, A98 (2020).
151. R. T. Garrod, E. Herbst, *A&A* **457**, 927–936 (2006).
152. R. T. Garrod, V. Wakelam, E. Herbst, *A&A* **467**, 1103–1115 (2007).
153. R. T. Garrod, S. L. Widicus Weaver, E. Herbst, *ApJ* **682**, 283–302 (2008).
154. W. D. Geppert *et al.*, *Faraday Discussions* **133**, 177 (2006).
155. P. A. Gerakines *et al.*, *A&A* **296**, 810 (1995).
156. G. Giardino *et al.*, *A&A* **463**, 275–288 (2007).
157. E. L. Gibb *et al.*, *ApJS* **151**, 35–73 (2004).
158. B. M. Giuliano *et al.*, *A&A* **592**, A81 (2016).
159. P. F. Goldsmith, W. D. Langer, *ApJ* **517**, 209–225 (1999).
160. M. Goto *et al.*, *arXiv e-prints* (2020).
161. R. J. Gould, E. E. Salpeter, *ApJ* **138**, 393 (1963).
162. L. V. Gramajo *et al.*, *AJ* **139**, 2504–2524 (2010).
163. T. Grassi *et al.*, *A&A* **643**, A155 (Nov. 2020).
164. R. O. Gray *et al.*, *AJ* **132**, 161–170 (2006).
165. G. M. Green *et al.*, *ApJ* **810**, 25 (2015).
166. M. J. Griffin *et al.*, *A&A* **518**, L3 (2010).
167. R. J. A. Grim *et al.*, *A&A* **243**, 473 (1991).
168. C. E. Groppi *et al.*, *ApJ* **670**, 489–498 (2007).
169. W. M. Grundy *et al.*, *Science* **367**, aay3705 (2020).
170. R. Güsten *et al.*, *A&A* **454**, L13–L16 (2006).
171. R. A. Gutermuth *et al.*, *ApJ* **673**, L151 (2008).
172. W. Hagen, L. J. Allamandola, J. M. Greenberg, *A&A* **86**, L3–L6 (1980).
173. G. Haro, *ApJ* **115**, 572 (1952).

174. J. Harris, B. Kasemo, *Surface Science* **105**, L281–L287 (1981).
175. D. Harsono *et al.*, *A&A* **562**, A77 (2014).
176. D. Harsono *et al.*, *Nature Astronomy* **2**, 646–651 (2018).
177. P. Hartigan, J. A. Graham, *AJ* **93**, 913 (1987).
178. P. Harvey *et al.*, *ApJ* **663**, 1149–1173 (2007).
179. T. I. Hasegawa, E. Herbst, *MNRAS* **263**, 589 (1993).
180. T. I. Hasegawa, E. Herbst, C. M. Leung, *ApJS* **82**, 167 (1992).
181. T. Hassenkam *et al.*, *Nature* **548**, 78–81 (2017).
182. T. J. Haworth *et al.*, *MNRAS* **501**, 3502–3514 (2021).
183. C. Heiles, H. J. Habing, *A&AS* **14**, 1 (1974).
184. T. T. Helfer *et al.*, *ApJS* **145**, 259–327 (2003).
185. T. Henning, *ARA&A* **48**, 21–46 (2010).
186. T. Henning, G. Meeus, in *Physical Processes in Circumstellar Disks around Young Stars* (Garcia, Paulo J. V., 2011), pp. 114–148.
187. G. H. Herbig, *Vistas in Astronomy* **8**, 109–125 (1966).
188. G. H. Herbig, *ApJ* **111**, 11 (1950).
189. G. H. Herbig, *ApJS* **4**, 337 (1960).
190. E. Herbst, W. Klemperer, *ApJ* **185**, 505–534 (1973).
191. E. Herbst, C. M. Leung, *ApJS* **69**, 271 (1989).
192. E. Herbst, E. F. van Dishoeck, *ARA&A* **47**, 427–480 (2009).
193. G. J. Herczeg *et al.*, *ApJ* **849**, 43 (2017).
194. G. J. Herczeg *et al.*, *ApJ* **878**, 111 (2019).
195. J. Hernández *et al.*, *ApJ* **662**, 1067–1081 (2007).
196. J. Hernández *et al.*, *ApJ* **707**, 705–715 (2009).
197. J. Hernández *et al.*, *ApJ* **794**, 36 (2014).
198. M. Heyer, T. M. Dame, *ARA&A* **53**, 583–629 (2015).
199. C. N. Hinshelwood, in (Oxford University Press, 1940), pp. 36–39.
200. P. T. P. Ho, J. M. Moran, K. Y. Lo, *ApJ* **616**, L1–L6 (2004).
201. S. Hoban *et al.*, *Icarus* **105**, 548–556 (1993).
202. J. A. Högbom, *A&AS* **15**, 417 (1974).
203. D. J. Hollenbach, A. G. G. M. Tielens, *Reviews of Modern Physics* **71**, 173–230 (1999).
204. D. Hollenbach, C. F. McKee, *ApJ* **342**, 306 (1989).
205. D. Hollenbach, E. E. Salpeter, *ApJ* **163**, 155 (1971).
206. M. Honda *et al.*, *ApJ* **690**, L110–L113 (2009).
207. D. M. Hudgins *et al.*, *ApJS* **86**, 713–870 (1993).
208. C. L. H. Hull *et al.*, *ApJ* **847**, 92 (2017).
209. R. L. Hurt, M. Barsony, *ApJ* **460**, L45 (1996).
210. S. Ioppolo *et al.*, *ApJ* **686**, 1474–1479 (2008).
211. S. Ioppolo *et al.*, *MNRAS* **413**, 2281–2287 (2011).
212. S. Ioppolo *et al.*, *A&A* **646**, A172 (2021).
213. M. Ishii *et al.*, *AJ* **124**, 2790–2798 (2002).
214. J. H. Jeans, *Philosophical Transactions of the Royal Society of London Series A* **199**, 1–53 (1902).
215. R. D. Jeffries, *MNRAS* **376**, 1109–1119 (2007).
216. A. Jiménez-Escobar *et al.*, *ApJ* **820**, 25 (2016).
217. A. Jiménez-Escobar *et al.*, *ApJ* **868**, 73 (2018).

218. I. Jiménez-Serra *et al.*, *A&A* **482**, 549–559 (2008).
219. I. Jiménez-Serra *et al.*, *Astrobiology* **20**, 1048–1066 (2020).
220. D. Johnstone *et al.*, *ApJ* **559**, 307–317 (2001).
221. J. K. Jørgensen *et al.*, *A&A* **415**, 1021–1037 (2004).
222. J. K. Jørgensen *et al.*, *A&A* **595**, A117 (2016).
223. J. K. Jørgensen, A. Belloche, R. T. Garrod, *ARA&A* **58**, 727–778 (2020).
224. G. Jungclaus *et al.*, *Meteoritics* **11**, 231–237 (1976).
225. J. Kauffmann *et al.*, *A&A* **487**, 993–1017 (2008).
226. J. V. Keane *et al.*, *A&A* **376**, 254–270 (2001).
227. M. Keppler *et al.*, *A&A* **617**, A44 (2018).
228. G. Kim *et al.*, *ApJS* **249**, 33 (2020).
229. R. F. Knacke *et al.*, *ApJ* **179**, 847–854 (1973).
230. C. Knez *et al.*, *ApJ* **635**, L145–L148 (2005).
231. J. Koda *et al.*, *ApJS* **193**, 19 (2011).
232. K. W. Kolasinski, in (Wiley, J. & Sons Ltd., Chichester, England, 1st Ed., 2002).
233. V. Könyves *et al.*, *A&A* **584**, A91 (2015).
234. M. Kounkel, *ApJ* **902**, 122 (2020).
235. M. Kounkel *et al.*, *AJ* **156**, 84 (2018).
236. L. E. Kristensen, M. M. Dunham, *A&A* **618**, A158 (2018).
237. L. E. Kristensen *et al.*, *A&A* **516**, A57 (2010).
238. M. Kuffmeier, B. Zhao, P. Caselli, *A&A* **639**, A86 (2020).
239. M. Kuffmeier, T. Haugbølle, Å. Nordlund, *ApJ* **846**, 7 (2017).
240. Y. Kurono, K.-I. Morita, T. Kamazaki, *PASJ* **61**, 873 (2009).
241. C. J. Lada, J. H. Black, *ApJ* **203**, L75–L79 (1976).
242. C. J. Lada, in *Star Forming Regions* (Peimbert, Manuel and Jugaku, Jun, 1987), vol. 115, p. 1.
243. E. F. Ladd, G. A. Fuller, J. R. Deane, *ApJ* **495**, 871–890 (1998).
244. W. J. Lang *et al.*, *A&A* **357**, 1001–1012 (2000).
245. P. Langevin, *J. Phys. Theor. Appl.* **4**, 678 (1905).
246. I. Langmuir, *Trans. Faraday Soc.* **17**, 607–620 (1922).
247. B. Larsson *et al.*, *A&A* **363**, 253–268 (2000).
248. L. Le Roy *et al.*, *A&A* **583**, A1 (2015).
249. H. H. Lee *et al.*, *A&A* **311**, 690–707 (1996).
250. H.-T. Lee *et al.*, *ApJ* **624**, 808–820 (2005).
251. K. I. Lee *et al.*, *ApJ* **797**, 76 (2014).
252. K. Levenberg, *Quart. Appl. Math.* **2**, 164–168 (1944).
253. Y. Lin *et al.*, *ApJ* **840**, 22 (2017).
254. J. E. Lindberg, J. K. Jørgensen, *A&A* **548**, A24 (2012).
255. J. E. Lindberg *et al.*, *A&A* **584**, A28 (2015).
256. J. E. Lindberg *et al.*, *A&A* **566**, A74 (2014).
257. J. E. Lindberg *et al.*, *ApJ* **835**, 3 (2017).
258. H. Linnartz, S. Ioppolo, G. Fedoseev, *International Reviews in Physical Chemistry* **34**, 205–237 (2015).
259. T. Liu *et al.*, *ApJS* **222**, 7 (2016).
260. R. Lüst, A. Schlüter, *ZAp* **38**, 190 (1955).
261. M.-M. Mac Low, R. S. Klessen, *Reviews of Modern Physics* **76**, 125–194 (2004).
262. R. J. Maddalena, M. Morris, *ApJ* **323**, 179 (1987).

263. E. E. Mamajek, in *Exoplanets and Disks: Their Formation and Diversity* (Usuda, Tomonori, Tamura, Motohide, and Ishii, Miki, 2009), vol. 1158, pp. 3–10.

264. E. E. Mamajek, M. R. Meyer, J. Liebert, *AJ* **124**, 1670–1694 (2002).

265. S. Manigand *et al.*, *A&A* **635**, A48 (2020).

266. D. Marquardt, *J. Soc. Indust. Appl. Math.* **11**, 431–441 (1963).

267. R. Martín-Doménech, G. M. Muñoz Caro, G. A. Cruz-Díaz, *A&A* **589**, A107 (2016).

268. R. Martín-Doménech *et al.*, *ApJ* **880**, 130 (2019).

269. R. D. Mathieu, in *in Handbook of Star Forming Regions, Volume I. The Northern Sky* (Reipurth, B. ed, 2008), vol. 4, ASP Monographs, p. 757.

270. A. J. Maury *et al.*, *A&A* **621**, A76 (2019).

271. B. A. McGuire, *ApJS* **239**, 17 (2018).

272. J. P. McMullin *et al.*, in *Astronomical Data Analysis Software and Systems XVI* (Shaw, R. A., Hill, F., and Bell, D. J., 2007), vol. 376, p. 127.

273. J. P. McMullin *et al.*, *ApJ* **424**, 222 (1994).

274. J. P. McMullin *et al.*, *ApJ* **536**, 845–856 (2000).

275. S. T. Megeath *et al.*, *AJ* **144**, 192 (2012).

276. S. T. Megeath *et al.*, *AJ* **151**, 5 (2016).

277. C. Meinert *et al.*, *Science* **352**, 208–212 (2016).

278. K. M. Menten *et al.*, *A&A* **474**, 515–520 (2007).

279. D. Mesa *et al.*, *A&A* **624**, A4 (2019).

280. L. Mestel, *MNRAS* **138**, 359 (1968).

281. O. Miettinen *et al.*, *A&A* **486**, 799–806 (2008).

282. M. Minissale *et al.*, *A&A* **585**, A24 (2016).

283. M. Minissale *et al.*, *MNRAS* **458**, 2953–2961 (2016).

284. N. Miyauchi *et al.*, *Chemical Physics Letters* **456**, 27–30 (2008).

285. P. Modica, M. E. Palumbo, G. Strazzulla, *Planet. Space Sci.* **73**, 425–429 (2012).

286. S. J. Mojzsis *et al.*, *Nature* **384**, 55–59 (1996).

287. L. K. Morgan *et al.*, *A&A* **477**, 557–571 (2008).

288. J. C. Mottram *et al.*, *A&A* **600**, A99 (2017).

289. J. Moultaka *et al.*, *A&A* **425**, 529–542 (2004).

290. G. M. Muñoz Caro *et al.*, *ACS Earth and Space Chemistry* **3**, 2138–2157 (2019).

291. H. S. P. Müller *et al.*, *A&A* **370**, L49–L52 (2001).

292. M. J. Mumma, S. B. Charnley, *ARA&A* **49**, 471–524 (2011).

293. K. Murakawa, M. Tamura, T. Nagata, *ApJS* **128**, 603–613 (2000).

294. P. Murdin, M. V. Penston, *MNRAS* **181**, 657 (1977).

295. N. M. Murillo *et al.*, *A&A* **592**, A56 (2016).

296. P. C. Myers, E. F. Ladd, *ApJ* **413**, L47 (1993).

297. P. C. Myers, R. A. Linke, P. J. Benson, *ApJ* **264**, 517–537 (1983).

298. P. C. Myers *et al.*, *ApJ* **324**, 907 (1988).

299. P. C. Myers, *ApJ* **700**, 1609–1625 (2009).

300. F. Nakamura *et al.*, *ApJ* **837**, 154 (2017).

301. J. Nelder, R. Mead, *The Computer Journal* **7**, 308 (1965).

302. D. A. Neufeld, A. Dalgarno, *ApJ* **340**, 869 (1989).

303. R. Neuhäuser, J. Forbrich, in *Handbook of Star Forming Regions, Volume II* (Reipurth, B., 2008), vol. 5, p. 735.

304. R. Neuhäuser *et al.*, *A&AS* **146**, 323–347 (2000).

305. B. Nisini *et al.*, *A&A* **518**, L120 (2010).

306. J. A. Noble *et al.*, *MNRAS* **421**, 768–779 (2012).
307. J. A. Noble *et al.*, *ApJ* **775**, 85 (2013).
308. J. A. Noble *et al.*, *Monthly Notices of the Royal Astronomical Society* **467**, 4753–4762 (2017).
309. J. A. Noble, PhD thesis, Dept. of Physics, Univ. of Strathclyde, 2011.
310. M. Nuevo, G. Cooper, S. A. Sandford, *Nature Communications* **9**, 5276 (2018).
311. D. J. Nutter, D. Ward-Thompson, P. André, *MNRAS* **357**, 975–982 (2005).
312. K. I. Öberg, S. Bottinelli, E. F. van Dishoeck, *A&A* **494**, L13–L16 (2009).
313. K. I. Öberg *et al.*, *ApJ* **621**, L33–L36 (2005).
314. K. I. Öberg *et al.*, *A&A* **504**, 891–913 (2009).
315. K. I. Öberg *et al.*, *ApJ* **740**, 109 (2011).
316. K. I. Öberg, *Chemical Reviews* **116**, 9631–9663 (2016).
317. K. I. Öberg, E. A. Bergin, *Phys. Rep.* **893**, 1–48 (2021).
318. K. I. Öberg, R. Murray-Clay, E. A. Bergin, *ApJ* **743**, L16 (2011).
319. K. I. Öberg *et al.*, *ApJ* **740**, 14 (2011).
320. T. Oka, *Proceedings of the National Academy of Science* **103**, 12235–12242 (2006).
321. G. N. Ortiz-León *et al.*, *ApJ* **869**, L33 (2018).
322. V. Ossenkopf, T. Henning, *A&A* **291**, 943–959 (1994).
323. P. Padoan, Å. Nordlund, *ApJ* **576**, 870–879 (2002).
324. Y. J. Pendleton, A. G. G. M. Tielens, M. W. Werner, *ApJ* **349**, 107 (1990).
325. E. M. Penteado, C. Walsh, H. M. Cuppen, *ApJ* **844**, 71 (2017).
326. G. Perotti *et al.*, *A&A* **643**, A48 (2020).
327. G. Perotti *et al.*, *A&A* **650**, A168 (2021).
328. D. E. Peterson *et al.*, *ApJS* **194**, 43 (2011).
329. H. M. Pickett *et al.*, *J. Quant. Spectr. Rad. Transf.* **60**, 883–890 (1998).
330. J. B. Pickles, D. A. Williams, *Ap&SS* **52**, 443–452 (1977).
331. M. Planck, *Verhandl. Dtsch. phys. Ges.* **2**, 202 (1900).
332. D. Polychroni *et al.*, *ApJ* **777**, L33 (2013).
333. K. M. Pontoppidan, *A&A* **453**, L47–L50 (2006).
334. K. M. Pontoppidan, S. M. Blevins, *Faraday Discussions* **168**, 49–60 (2014).
335. K. M. Pontoppidan, E. F. van Dishoeck, E. Dartois, *A&A* **426**, 925–940 (2004).
336. K. M. Pontoppidan *et al.*, *A&A* **408**, 981–1007 (2003).
337. K. M. Pontoppidan *et al.*, *A&A* **404**, L17–L20 (2003).
338. K. M. Pontoppidan *et al.*, *ApJ* **678**, 1005–1031 (2008).
339. K. M. Pontoppidan *et al.*, in *Protostars and Planets VI* (Beuther, Henrik et al., 2014), p. 363.
340. K. M. Pontoppidan *et al.*, *ApJ* **874**, 92 (2019).
341. M. S. Povich *et al.*, *ApJS* **209**, 31 (2013).
342. T. Preibisch, *A&A* **410**, 951–959 (2003).
343. T. Preibisch, *A&A* **428**, 569–577 (2004).
344. R. E. Pudritz, T. P. Ray, *Frontiers in Astronomy and Space Sciences* **6**, 54 (2019).
345. D. Qasim *et al.*, *A&A* **612**, A83 (2018).
346. D. Qasim *et al.*, *Nature Astronomy* **4**, 781–785 (2020).
347. S.-L. Qin, Y.-F. Wu, *Chinese J. Astron. Astrophys.* **3**, 69–74 (2003).
348. D. Rabli, D. R. Flower, *MNRAS* **406**, 95–101 (2010).
349. F. R. S. Rayleigh, *XXXI. Investigations in optics, with special reference to the spectroscope*, 1879.
350. P. Redondo, C. Barrientos, A. Largo, *ApJ* **836**, 240 (2017).

351. P. Redondo *et al.*, *A&A* **603**, A139 (2017).
352. B. Reipurth, *VizieR Online Data Catalog*, V/104 (2000).
353. B. Reipurth, J. Bally, *ARA&A* **39**, 403–455 (2001).
354. B. Reipurth, P. Friberg, *MNRAS* **501**, 5938–5947 (2021).
355. V. M. Rivilla *et al.*, *MNRAS* **483**, L114–L119 (2019).
356. H. Roberts, T. J. Millar, *A&A* **361**, 388–398 (2000).
357. T. P. Robitaille, *A&A* **600**, A11 (2017).
358. T. P. Robitaille *et al.*, *ApJS* **169**, 328–352 (2007).
359. T. P. Robitaille *et al.*, *ApJS* **167**, 256–285 (2006).
360. W. R. M. Rocha, S. Pilling, *ApJ* **803**, 18 (2015).
361. K. Rohlfs, T. L. Wilson, *Tools of Radio Astronomy* (Springer Verlag, 1996).
362. G. S. Rossano, *AJ* **83**, 234–240 (1978).
363. L. S. Rothman *et al.*, *Appl. Opt.* **26**, 4058–4097 (1987).
364. M. Rubin *et al.*, *MNRAS* **489**, 594–607 (2019).
365. D. P. Ruffle, E. Herbst, *MNRAS* **322**, 770–778 (2001).
366. D. P. Ruffle, E. Herbst, *MNRAS* **324**, 1054–1062 (2001).
367. D. Rumble *et al.*, *MNRAS* **448**, 1551–1573 (2015).
368. M. Sahan, L. M. Haffner, *AJ* **151**, 147 (2016).
369. G. Santangelo *et al.*, *A&A* **538**, A45 (2012).
370. S. L. Schnee *et al.*, *ApJ* **634**, 442–450 (2005).
371. S. Schneider, B. G. Elmegreen, *ApJS* **41**, 87–95 (1979).
372. F. L. Schöier *et al.*, *A&A* **390**, 1001–1021 (2002).
373. F. L. Schöier *et al.*, *A&A* **432**, 369–379 (2005).
374. F. L. Schöier *et al.*, *A&A* **454**, L67–L70 (2006).
375. W. A. Schutte *et al.*, *A&A* **343**, 966–976 (1999).
376. D. M. Segura-Cox *et al.*, *ApJ* **866**, 161 (2018).
377. D. M. Segura-Cox *et al.*, *Nature* **586**, 228–231 (2020).
378. R. J. Shannon *et al.*, *Nature Chemistry* **5**, 745–749 (2013).
379. R. J. Shannon *et al.*, *RSC Advances* **4**, 26342–26353 (2014).
380. S. Sharpless, *ApJS* **4**, 257 (1959).
381. T. Shimonishi *et al.*, *ApJ* **855**, 27 (2018).
382. F. H. Shu, *ApJ* **214**, 488–497 (1977).
383. M. A. J. Simons, T. Lamberts, H. M. Cuppen, *A&A* **634**, A52 (2020).
384. D. Skouteris *et al.*, *ApJ* **854**, 135 (2018).
385. M. F. Skrutskie *et al.*, *AJ* **131**, 1163–1183 (2006).
386. L. Song, J. Kästner, *ApJ* **850**, 118 (2017).
387. S. Spezzano *et al.*, *A&A* **643**, A60 (2020).
388. F. Stahler, S. W. Palla, in *The Formation of Stars* (Wiley-VCH Verlag GmbG & Co, 2004).
389. S. Stanimirovic, in *Single-Dish Radio Astronomy: Techniques and Applications* (Stanimirovic, Snezana et al., 2002), vol. 278, pp. 375–396.
390. T. P. Stecher, D. A. Williams, *Astrophys. Lett.* **4**, 99 (1969).
391. D. P. Stevenson, D. O. Schissler, *J. Chem. Phys.* **29**, 282 (1958).
392. S. E. Strom, G. L. Grasdalen, K. M. Strom, *ApJ* **191**, 111–142 (1974).
393. K. Sugitani, Y. Fukui, K. Ogura, *ApJS* **77**, 59 (1991).
394. A. N. Suutarinen *et al.*, *MNRAS* **440**, 1844–1855 (2014).

395. A. Suutarinen, http://oro.open.ac.uk/61309/, PhD thesis, Dept. of Physics, The Open University, 2015.
396. A. Suutarinen, *omnifit v0.1*, https://doi.org/10.5281/zenodo.29354, 2015.
397. K. N. R. Taylor, J. W. V. Storey, *MNRAS* **209**, 5P–10 (1984).
398. S. Terebey, F. H. Shu, P. Cassen, *ApJ* **286**, 529–551 (1984).
399. J. Terwisscha van Scheltinga *et al.*, *A&A* **611**, A35 (2018).
400. W.-F. Thi *et al.*, *A&A* **449**, 251–265 (2006).
401. A. G. G. M. Tielens, W. Hagen, *A&A* **114**, 245–260 (1982).
402. J. J. Tobin *et al.*, *Nature* **492**, 83–85 (2012).
403. J. J. Tobin *et al.*, *ApJ* **805**, 125 (2015).
404. W. Tscharnuter, *A&A* **39**, 207 (1975).
405. B. E. Turner, *ApJ* **501**, 731–748 (1998).
406. Ł. Tychoniec *et al.*, *A&A* **632**, A101 (2019).
407. Ł. Tychoniec *et al.*, *A&A* **640**, A19 (2020).
408. M. Vasta *et al.*, *A&A* **537**, A98 (2012).
409. A. I. Vasyunin, E. Herbst, *ApJ* **769**, 34 (2013).
410. A. I. Vasyunin *et al.*, *ApJ* **842**, 33 (2017).
411. F. Vazart *et al.*, *MNRAS* **499**, 5547–5561 (2020).
412. R. Visser, S. D. Doty, E. F. van Dishoeck, *A&A* **534**, A132 (2011).
413. R. Visser *et al.*, *A&A* **495**, 881–897 (2009).
414. S. N. Vogel *et al.*, *ApJ* **283**, 655–667 (1984).
415. C. M. Wade, *AJ* **62**, 148 (1957).
416. A. F. Wagner, M. M. Graff, *ApJ* **317**, 423 (1987).
417. V. Wakelam *et al.*, *Molecular Astrophysics* **9**, 1–36 (2017).
418. C. Walsh *et al.*, *ApJ* **823**, L10 (2016).
419. F. M. Walter *et al.*, *Mem. Soc. Astron. Italiana* **68**, 1081–1088 (1997).
420. H. Wang *et al.*, *ApJ* **617**, 1191–1203 (2004).
421. N. Watanabe, A. Kouchi, *ApJ* **571**, L173–L176 (2002).
422. Y. Watanabe *et al.*, *ApJ* **745**, 126 (2012).
423. W. D. Watson, E. E. Salpeter, *ApJ* **174**, 321 (1972).
424. W. D. Watson, *ApJ* **183**, L17 (1973).
425. J. C. Weingartner, B. T. Draine, *ApJ* **548**, 296–309 (2001).
426. A. Weiß *et al.*, *A&A* **365**, 571–587 (2001).
427. M. S. Westley *et al.*, *Nature* **373**, 405–407 (1995).
428. G. J. White, M. M. Casali, C. Eiroa, *A&A* **298**, 594 (1995).
429. B. A. Whitney *et al.*, *ApJ* **598**, 1079–1099 (2003).
430. D. C. B. Whittet *et al.*, *ApJ* **742**, 28 (2011).
431. D. A. Williams, S. Viti, *Observational Molecular Astronomy: Exploring the Universe Using Molecular Line Emissions* (Cambridge University Press, 2013).
432. J. P. Williams, W. M. J. Best, *ApJ* **788**, 59 (2014).
433. J. P. Williams, L. A. Cieza, *ARA&A* **49**, 67–117 (2011).
434. T. L. Wilson, *Reports on Progress in Physics* **62**, 143–185 (1999).
435. T. L. Wilson, F. Matteucci, *A&A Rev.* **4**, 1–33 (1992).
436. A. J. Winter *et al.*, *MNRAS* **491**, 903–922 (2020).
437. M. G. Wolfire, D. Hollenbach, A. G. G. M. Tielens, *ApJ* **344**, 770 (1989).
438. E. L. Wright *et al.*, *AJ* **140**, 1868–1881 (2010).

439. B. Yang *et al.*, *ApJ* **718**, 1062–1069 (2010).
440. H.-W. Yi *et al.*, *ApJS* **236**, 51 (2018).
441. H.-W. Yi *et al.*, *arXiv e-prints*, arXiv:2103.03499 (2021).
442. L. Zamirri *et al.*, *MNRAS* **480**, 1427–1444 (2018).
443. G. Zasowski *et al.*, *ApJ* **694**, 459–478 (2009).
444. F. Zernike, *Physica* **5**, 785–795 (1938).
445. C. Y. Zhang *et al.*, *A&A* **218**, 231–240 (1989).
446. C. Zhang *et al.*, *MNRAS* **497**, 793–808 (2020).
447. Z.-Y. Zhang *et al.*, *Nature* **558**, 260–263 (2018).
448. C. Zucker *et al.*, *ApJ* **879**, 125 (2019).
449. C. Zucker *et al.*, *A&A* **633**, A51 (2020).
450. P. H. van Cittert, *Physica* **1**, 201–210 (1934).
451. E. F. van Dishoeck, in *Millimetre and Submillimetre Astronomy* (Wolstencroft, R. D. and Burton, W. B., 1988), vol. 147, p. 117.
452. E. F. van Dishoeck, J. H. Black, *ApJS* **62**, 109 (1986).
453. E. F. van Dishoeck, E. A. Bergin, *arXiv e-prints* (2020).
454. E. F. van Dishoeck, J. H. Black, *ApJ* **334**, 771 (1988).
455. E. F. van Dishoeck, G. A. Blake, *ARA&A* **36**, 317–368 (1998).
456. M. L. van Gelder *et al.*, *A&A* **639**, A87 (2020).
457. S. E. van Terwisga *et al.*, *A&A* **640**, A27 (2020).
458. H. C. van de Hulst, *Recherches Astronomiques de l'Observatoire d'Utrecht* **11**, 2.i–2 (1946).
459. M. L. R. van 't Hoff *et al.*, *A&A* **599**, A101 (2017).
460. M. L. R. van 't Hoff *et al.*, *ApJ* **864**, L23 (2018).